On the Use of Clarke Transformation for the Time-Domain Analysis of Asymmetrical Faults in Three-Phase Power Systems

Diego Bellan *

Posted Date: 7 May 2026

doi: 10.20944/preprints202605.0003.v2

Keywords: Clarke transformation; fault analysis; power quality; power system analysis; space vectors; time-domain analysis; transient analysis; voltage sags

 doi:10.20944/preprints202605.0003.v2

Article

On the Use of Clarke Transformation for the Time-Domain Analysis of Asymmetrical Faults in Three-Phase Power Systems

Diego Bellan

Department of Electronics, Information and Bioengineering, Politecnico di Milano, Milan, Italy; diego.bellan@polimi.it

Abstract

This work deals with the time-domain analysis of asymmetrical faults in three-phase systems. Conventional three-phase analysis provides steady-state solutions for asymmetrical faults. Transient analysis, however, is usually performed by resorting either to oversimplified approximate circuits, or to numerical methods. In this paper, a rigorous analytical methodology based on the time-domain Clarke transformation is presented for the most common asymmetrical faults in three-phase systems. In particular, it is shown that asymmetrical faults result in circuit coupling in the Clarke equivalent circuits. Circuit representation of coupling is also derived in the paper. Coupled equivalent circuits allow rigorous analytical solution of transients in case of asymmetrical faults. The analytical results derived in the paper are validated through proper numerical simulation of faulted radial systems.

Keywords: Clarke transformation; fault analysis; power quality; power system analysis; space vectors; time-domain analysis; transient analysis; voltage sags

1. Introduction

Transients are a common phenomenon in three-phase power systems. Indeed, transients can be due to external causes like lightning, or internal intended/unintended causes like system operations and faults. Transient analysys is of paramount importance in modern power systems because typically they imply temporary overcurrents and overvoltages that could lead to malfunctioning and damage of system components.

As far as faults are concerned, extensive literature can be found about steady-state analytical calculation of voltages/currents faults. Such conventional approaches are mainly based on a proper adaptation of the well-known Symmetrical Component Transformation (SCT) [1]. On the contrary, when time-domain analysis (i.e., transient analysis) is required, the related literature provides oversimplified and approximate analytical approaches, or the use of numerical tools [2,3]. Approximate analytical approaches are mainly based on the time domain analysis of positive sequence circuits obtained through the SCT, whereas many numerical tools nowadays are available such as the Electromagnetic Transient Program (EMTP). To the Author knowledge, however, a rigorous analytical approach for the transient analysis of asymmetrical faults specific to three-phase systems is still lacking.

This paper is based on the use of the Clarke transformation of three-phase variables and circuits [4–6]. In contrast to the SCT, operating in the phasor domain, the Clarke transformation operates in the time domain, therefore it seems a suitable tool for three-phase transient analysis. Actually, the main idea underlying the Clarke transformation is similar to the SCT. In fact, in case of system symmetry, the Clarke transformation provides three uncoupled time-domain circuits with variables called α, β, and zero. In case of system asymmetry, however, it was already shown in [5] that the three Clarke circuits can be coupled, depending on the kind of system asymmetry. Thus, as a general principle, in case of system asymmetry the oversimplified approach consisting in the transient

 doi:10.20944/preprints202605.0003.v2

analysis of only the positive sequence circuit is not correct. Instead, for each kind of asymmetrical fault, a proper circuit representation of coupling between Clarke circuits is needed to obtain the exact analytical time-domain solution.

Clarke transformation is also the basis for the definition of voltage/current space vectors [4–6]. A voltage/current space vector is a complex-valued time function where the real and the imaginary parts are given by the α and β components of a Clarke transformed voltage/current, respectively. In the ideal unfaulted case, the trajectory of voltage space vector on the complex plane is circular. On the contrary, in case of fault, the trajectory of the voltage space vector on the complex plane is elliptical, where the inclination angle of the ellipse allows the classification of the kind of fault [7–18]. Figure 1 shows the classification angles for single phase (S) and double phase (D) faults [18]. Notice that in [18] only the special case of steady-state single-phase fault was considered. In this paper, however, the transient solution through the Clarke transformation is proposed, and a more general fault condition is considered including asymmetrical double-phase and three-phase faults. Thus, the results derived in the paper allow also straightforward detection, classification and characterization of the kind of fault. Moreover, the impact of circuit parameters on the effectiveness of fault characterization can be readily performed.

The general methodology introduced in this paper can be outlined as follows. The main assumption is the three-phase symmetry of the system, apart from the fault section where fault constraints are typically asymmetrical. The symmetric part of the three-phase system is processed according to the Clarke transformation. Thus, three circuits, named α, β, and zero, with transformed topology and variables can be defined. The asymmetrical part, i.e., the fault section, is characterized by specific constraints on the phase variables, depending on the kind of fault (i.e., single/double/three-phase, grounded or ungrounded). The constraints on the phase variables, once Clarke transformed, become constraints on the α, β,0 variables at fault location. Through specific mathematical derivations it is shown that such constraints can be represented as proper circuit elements (mainly ideal transformers) coupling the α, β,0 circuits. Thanks to such simple equivalent circuits, the three-phase transient can be easily solved in the time domain for each specific kind of fault. It is worth highlighting that such approach is not approximate, but it provides the rigorous and exact analytical solution. Numerical simulations of transients in a three-phase radial system validate the correctness of the proposed analytical approach.

The paper is organized as follows. In Section 2, the Clarke transformation of variables and some topological aspects are recalled. In Section 3, the analytical derivations for the single-phase fault, double-phase asymmetrical grounded and ungrounded faults, and three-phase asymmetrical ungrounded fault, and the introduction of the related equivalent circuits, are presented in detail. Numerical validation of the derived analytical results and equivalent circuits is presented in Section 4 for a three-phase radial system. Finally, conclusions are presented in Section 5.

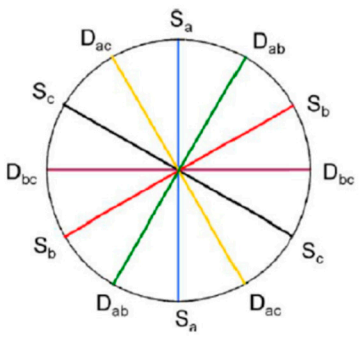

Figure 1. The voltage space-vector shows an elliptical behavior on the complex plane, where the inclination angle of the ellipse depends on the kind of fault. Single-phase faults ($S_{a,b,c}$) correspond to 0°, 60°, and 120°. Double-phase faults ($D_{ab,bc,ac}$) correspond to 30°, 90°, and 50° [18].

 doi:10.20944/preprints202605.0003.v2

2. Clarke Transformation and Three-Phase Circuit Analysis

Let us consider a column vector of time-domain phase voltages $\boldsymbol{v}_{abc} = [v_a \quad v_b \quad v_c]^T$. The Clarke transformation of $\boldsymbol{v}_{abc}$ is defined as, [4–6]:

$$\boldsymbol{v}_{\alpha\beta 0} = \begin{bmatrix} v_\alpha \\ v_\beta \\ v_0 \end{bmatrix} = \boldsymbol{T}\boldsymbol{v}_{abc} = \sqrt{\frac{2}{3}} \begin{bmatrix} 1 & -\frac{1}{2} & -\frac{1}{2} \\ 0 & \frac{\sqrt{3}}{2} & -\frac{\sqrt{3}}{2} \\ \frac{1}{\sqrt{2}} & \frac{1}{\sqrt{2}} & \frac{1}{\sqrt{2}} \end{bmatrix} \begin{bmatrix} v_a \\ v_b \\ v_c \end{bmatrix} \tag{1}$$

where the transformation matrix $\boldsymbol{T}$ is defined in the power invariant form from the *abc* domain to the transformed $\alpha\beta 0$ domain. This property is of paramount importance in order to define consistent equivalent circuits in the Clarke domain.

The main feature of the Clarke transformation is the diagonalization of balanced three-phase component matrices. As a remarkable example, for a symmetrical mutual inductor in the time-domain we obtain [18]:

$$\begin{bmatrix} v_\alpha \\ v_\beta \\ v_0 \end{bmatrix} = \boldsymbol{T} \begin{bmatrix} L_{ph} & L_m & L_m \\ L_m & L_{ph} & L_m \\ L_m & L_m & L_{ph} \end{bmatrix} \boldsymbol{T}^{-1} \frac{d}{dt} \begin{bmatrix} i_\alpha \\ i_\beta \\ i_0 \end{bmatrix} =$$

$$= \begin{bmatrix} L_{ph} - L_m & 0 & 0 \\ 0 & L_{ph} - L_m & 0 \\ 0 & 0 & L_{ph} + 2L_m \end{bmatrix} \frac{d}{dt} \begin{bmatrix} i_\alpha \\ i_\beta \\ i_0 \end{bmatrix} =$$

$$= \begin{bmatrix} L_\alpha & 0 & 0 \\ 0 & L_\beta & 0 \\ 0 & 0 & L_0 \end{bmatrix} \frac{d}{dt} \begin{bmatrix} i_\alpha \\ i_\beta \\ i_0 \end{bmatrix} \tag{2}$$

Thus, three uncoupled equations were obtained in (2). Moreover, by considering that $L_\alpha = L_\beta$, the first two equations can be combined in one complex equation as:

$$\bar{v} = v_\alpha + jv_\beta = L\frac{d}{dt}\left(i_\alpha + ji_\beta\right) = L\frac{d}{dt}\bar{\imath} \tag{3}$$

where the voltage/current space vectors $\bar{v}$ and $\bar{\imath}$ have been introduced.

In case of a three-phase sinusoidal voltage source with phase voltages $\boldsymbol{e} = [e_a \quad e_b \quad e_c]^T$, by using the Clarke transformation we obtain the following space vector:

$$\bar{e} = e_\alpha + je_\beta = E_p e^{j\omega t} + E_n^* e^{-j\omega t} \tag{4}$$

where E_p and E_n are the positive/negative sequence components provided by the phasor Symmetrical Component Transformation (SCT) [17,18]:

$$\boldsymbol{E}_S = \begin{bmatrix} E_p \\ E_n \\ E_0 \end{bmatrix} = \frac{1}{\sqrt{3}} \begin{bmatrix} 1 & a & a^2 \\ 1 & a^2 & a \\ 1 & 1 & 1 \end{bmatrix} \begin{bmatrix} E_a \\ E_b \\ E_c \end{bmatrix} = \boldsymbol{S}\boldsymbol{E} \tag{5}$$

where $a = \exp(j\,2\pi/3)$, and the transformation matrix $\boldsymbol{S}$ is defined in its power invariant form such that $\boldsymbol{S}^{-1} = \boldsymbol{S}^{*T}$.

Under sinusoidal steady-state, the trajectory of the space vector $\bar{e}$ is elliptical, and the semi-major axis r_M, the semi-minor axis r_m, and inclination angle φ, are given by [17,18]:

$$r_M = |E_p| + |E_n^*| \tag{6}$$

$$r_m = \left||E_p| - |E_n^*|\right| \tag{7}$$

$$\varphi = \frac{1}{2}\left[arg(E_p) + arg(E_n^*)\right] \tag{8}$$

Clarke equivalent circuits in the $\alpha\beta 0$ variables can be obtained by transforming three-phase components as in (2), and by transforming three-phase symmetrical connections. The most common

 doi:10.20944/preprints202605.0003.v2

three-phase connections are the star connections, where the star center can be either non-accessible or accessible to connect the three-phase system to single-phase networks [18].

2.1. Star Connection with Non-Accessible Center

Figure 2 shows a star connection with non-accessible star center. By assuming a reference terminal *G* valid for the whole three-phase system, the star connection can be considered as a three-port network characterized by the following independent relationships:

$$v_a = v_b, \quad v_b = v_c, \quad i_a + i_b + i_c = 0 \tag{9}$$

By using (9) in the Clarke transformation (1), we obtain:

$$v_\alpha = v_\beta = 0 \tag{10}$$

$$i_0 = 0 \tag{11}$$

i.e., the star connection with a non-accessible center is equivalent to a short circuit in the $\alpha\beta$ domains, and an open circuit in the 0 domain.

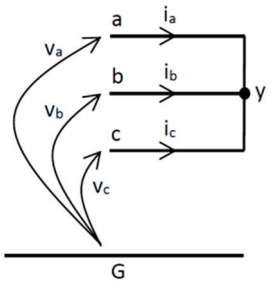

Figure 2. Star connection with non-accessible center [18].

2.2. Star Connection with Accessible Center

Figure 3 shows a star connection with accessible star center. The star center is normally used to connect the three-phase system to a single-phase circuit. This connection can be treated as a four-port network whose independent relationships are given by:

$$v_a = v_y, \quad v_b = v_y, \quad v_c = v_y, \quad i_a + i_b + i_c = i_y \tag{12}$$

By using (12) into the Clarke transformation (1) we obtain that this kind of connection is a short circuit in the $\alpha\beta$ domains, whereas in the 0 domain:

$$v_0 = \sqrt{3} v_y \tag{13}$$

$$i_0 = \frac{1}{\sqrt{3}} i_y \tag{14}$$

i.e., the interconnection between the 0 (three-phase) domain and the single-phase domain can be represented as an ideal transformer with turn ratio $\sqrt{3}$ (see Figure 4). The well-known properties of ideal transformers can be readily used to analyze circuits in the 0 domain and the interconnections with single-phase circuits.

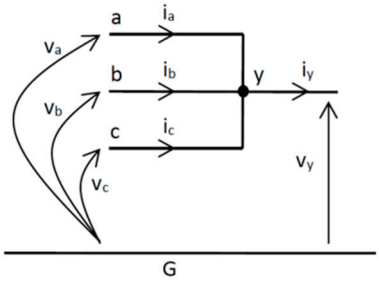

Figure 3. Star connection with accessible center [18].

 doi:10.20944/preprints202605.0003.v2

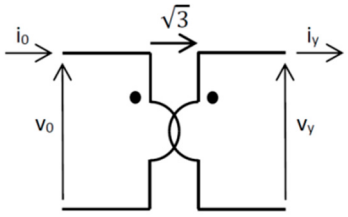

Figure 4. Zero-component equivalent circuit of a star connection with accessible center [18].

3. Time-Domain Analysis of Asymmetrical Faults

In this Section, the time-domain analysis of asymmetrical faults based on the Clarke transformation recalled in Section 2 will be developed. In particular, the following faults will be considered: a) single-phase faults, b) double-phase asymmetrical grounded and ungrounded faults, c) three-phase asymmetrical ungrounded faults.

Figure 5 shows the effect of Clarke transformation on the circuit variables. In the *abc* domain, phase voltages and currents belonging to the symmetrical part of the three-phase circuit are coupled, whereas the asymmetrical fault can be usually represented as uncoupled phases constraints. On the contrary, after Clarke transformation, the $\alpha\beta0$ variables in the symmetrical portion of the three-phase circuit are uncoupled, whereas the asymmetrical fault constraints result in coupled $\alpha\beta0$ variables. Thus, the $\alpha\beta0$ circuits result in coupled circuits at the fault location only. The effect of the Clarke transformation is therefore to move the circuit coupling from the whole three-phase system (i.e., the left side in Figure 5) to the asymmetrical fault only (i.e., the right side in Figure 5).

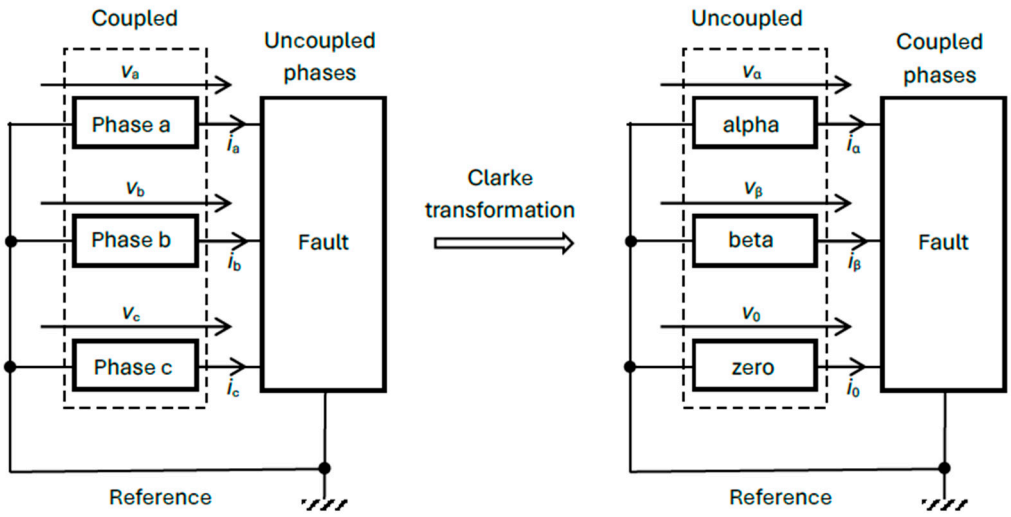

Figure 5. Clarke transformed variables at asymmetrical fault location.

3.1. Single-Phase Faults

A single-phase fault can be represented as in Figure 6 where only the switch corresponding to the faulted phase is closed. For the sake of simplicity, we assume a resistive fault R_f, however a generic *RLC* fault could be considered in the proposed time-domain analysis.

By assuming the faulted phase is phase *a*, the corresponding fault constraints on the phase variables are given by:

$$v_a = R_f i_a, \quad i_b = i_c = 0 \qquad (15)$$

 doi:10.20944/preprints202605.0003.v2

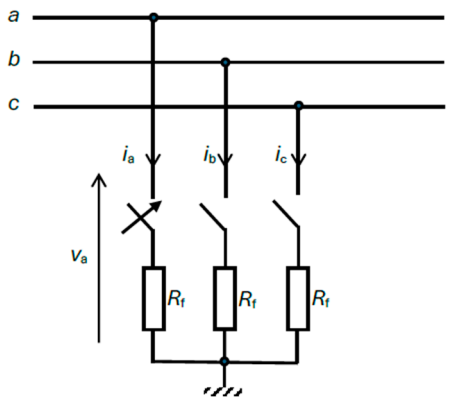

Figure 6. Single-phase fault implemented as the closure of one switch only. Fault of phase *a* is obtained by closing switch *a*.

By using (15) into the Clarke transformation defined in (1), we can readily obtain the αβ0 voltages and currents:

$$\boldsymbol{v}_{\alpha\beta 0} = \begin{bmatrix} v_\alpha \\ v_\beta \\ v_0 \end{bmatrix} = \sqrt{\frac{2}{3}} \begin{bmatrix} 1 & -\frac{1}{2} & -\frac{1}{2} \\ 0 & \frac{\sqrt{3}}{2} & -\frac{\sqrt{3}}{2} \\ \frac{1}{\sqrt{2}} & \frac{1}{\sqrt{2}} & \frac{1}{\sqrt{2}} \end{bmatrix} \begin{bmatrix} R_f i_a \\ v_b \\ v_c \end{bmatrix} = \sqrt{\frac{2}{3}} \begin{bmatrix} R_f i_a - \frac{v_b + v_c}{2} \\ \sqrt{3}\frac{v_b - v_c}{2} \\ \frac{R_f i_a + v_b + v_c}{\sqrt{2}} \end{bmatrix} \tag{16}$$

$$\boldsymbol{i}_{\alpha\beta 0} = \begin{bmatrix} i_\alpha \\ i_\beta \\ i_0 \end{bmatrix} = \sqrt{\frac{2}{3}} \begin{bmatrix} 1 & -\frac{1}{2} & -\frac{1}{2} \\ 0 & \frac{\sqrt{3}}{2} & -\frac{\sqrt{3}}{2} \\ \frac{1}{\sqrt{2}} & \frac{1}{\sqrt{2}} & \frac{1}{\sqrt{2}} \end{bmatrix} \begin{bmatrix} i_a \\ 0 \\ 0 \end{bmatrix} = \sqrt{\frac{2}{3}} \begin{bmatrix} i_a \\ 0 \\ \frac{1}{\sqrt{2}} i_a \end{bmatrix} \tag{17}$$

From (17) we observe that $i_\beta = 0$, i.e., β is an open circuit. Moreover:

$$i_0 = \frac{1}{\sqrt{2}} i_\alpha \tag{18}$$

By taking into account (17) into (16), for the α and 0 circuits we obtain:

$$v_\alpha = R_f i_\alpha - \frac{v_b + v_c}{\sqrt{6}} \tag{19}$$

$$v_0 = R_f i_0 + \frac{v_b + v_c}{\sqrt{3}} \tag{20}$$

Thus, from (18)-(20) we can readily obtain the circuit representation of coupling between α and 0 circuits through an ideal transformer with turn ratio $n = -1/\sqrt{2}$ as in Figure 7 where the open β circuit is also represented.

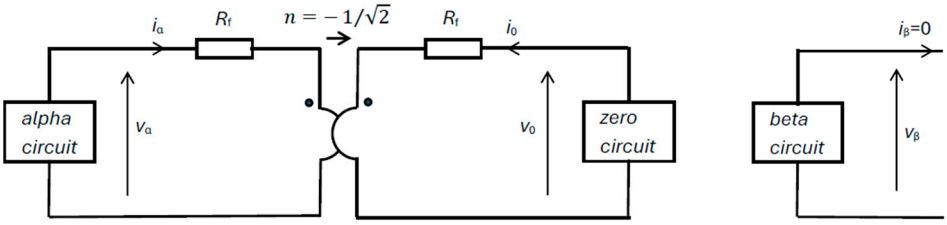

Figure 7. Clarke circuit representation of single-phase fault.

Notice that, according to the space vector definition (3), the β component of the voltage remains in a steady state, whereas the transient of the α component is affected by the coupling with the 0 circuit. As far as the current space vector is considered, we can observe that its β component is zero. Thus, the current transient is fully described by the α component of the current space vector, affected by the coupling with the 0 circuit.

 doi:10.20944/preprints202605.0003.v2

Finally, once the αβ0 circuits in Figure 7 are solved, the phase *abc* variables at fault location can be recovered through the inverse Clarke transformation. As far as the voltages are concerned, we obtain:

$$\boldsymbol{v}_{abc} = \begin{bmatrix} v_a \\ v_b \\ v_c \end{bmatrix} = \sqrt{\frac{2}{3}} \begin{bmatrix} 1 & 0 & \frac{1}{\sqrt{2}} \\ -\frac{1}{2} & \frac{\sqrt{3}}{2} & \frac{1}{\sqrt{2}} \\ -\frac{1}{2} & -\frac{\sqrt{3}}{2} & \frac{1}{\sqrt{2}} \end{bmatrix} \begin{bmatrix} v_\alpha \\ v_\beta \\ v_0 \end{bmatrix} = \sqrt{\frac{2}{3}} \begin{bmatrix} \mathrm{Re}\{\bar{v}\} + \frac{1}{\sqrt{2}} v_0 \\ \mathrm{Re}\{a^2 \bar{v}\} + \frac{1}{\sqrt{2}} v_0 \\ \mathrm{Re}\{a \bar{v}\} + \frac{1}{\sqrt{2}} v_0 \end{bmatrix} \tag{21}$$

where $\bar{v}$ is the space vector defined in (3), $\mathrm{Re}\{\cdot\}$ takes the real part, and $a = e^{j\frac{2\pi}{3}}$.

As far as the *abc* currents are considered, in this case only i_a is different from zero. From (17) we readily obtain:

$$i_a = \sqrt{\frac{3}{2}} i_\alpha = \sqrt{3} i_0 \tag{22}$$

3.2. Double-Phase Faults

Double-phase faults involve two phases and, possibly, the ground. In the general case, a double-phase fault can be represented as in Figure 8 where only two switches are closed. By closing the switches *b* and *c*, the corresponding constraints on the phase variables are given by:

$$i_a = 0, \quad v_b = R_{f1} i_b + R_{f2}(i_b + i_c), \quad v_c = R_{f1} i_c + R_{f2}(i_b + i_c) \tag{23}$$

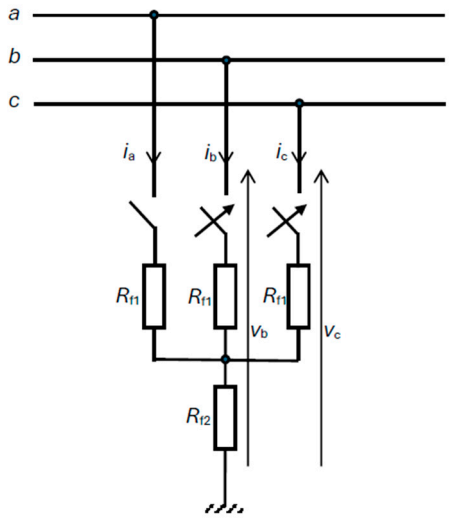

Figure 8. Circuit representation of double-phase grounded faults. By closing only the switches *b* and *c* the corresponding two phases are involved in the fault.

By using (23) into the Clarke transformation defined in (1), we can readily obtain the αβ0 voltages and currents:

$$\boldsymbol{v}_{\alpha\beta 0} = \begin{bmatrix} v_\alpha \\ v_\beta \\ v_0 \end{bmatrix} = \sqrt{\frac{2}{3}} \begin{bmatrix} 1 & -\frac{1}{2} & -\frac{1}{2} \\ 0 & \frac{\sqrt{3}}{2} & -\frac{\sqrt{3}}{2} \\ \frac{1}{\sqrt{2}} & \frac{1}{\sqrt{2}} & \frac{1}{\sqrt{2}} \end{bmatrix} \begin{bmatrix} v_a \\ R_{f1} i_b + R_{f2}(i_b + i_c) \\ R_{f1} i_c + R_{f2}(i_b + i_c) \end{bmatrix} =$$

$$= \sqrt{\frac{2}{3}} \begin{bmatrix} v_a - \frac{1}{2}(R_{f1} + 2R_{f2})(i_b + i_c) \\ \frac{\sqrt{3}}{2} R_{f1}(i_b - i_c) \\ \frac{1}{\sqrt{2}}\left[v_a + (R_{f1} + 2R_{f2})(i_b + i_c)\right] \end{bmatrix} \tag{24}$$

 doi:10.20944/preprints202605.0003.v2

$$\boldsymbol{i}_{\alpha\beta 0} = \begin{bmatrix} i_\alpha \\ i_\beta \\ i_0 \end{bmatrix} = \sqrt{\frac{2}{3}} \begin{bmatrix} 1 & -\frac{1}{2} & -\frac{1}{2} \\ 0 & \frac{\sqrt{3}}{2} & -\frac{\sqrt{3}}{2} \\ \frac{1}{\sqrt{2}} & \frac{1}{\sqrt{2}} & \frac{1}{\sqrt{2}} \end{bmatrix} \begin{bmatrix} 0 \\ i_b \\ i_c \end{bmatrix} = \sqrt{\frac{2}{3}} \begin{bmatrix} -\frac{1}{2}(i_b + i_c) \\ \frac{\sqrt{3}}{2}(i_b - i_c) \\ \frac{1}{\sqrt{2}}(i_b + i_c) \end{bmatrix} \quad (25)$$

From (24) and (25) with simple algebra we obtain:

$$i_0 = -\sqrt{2} i_\alpha \quad (26)$$

and

$$v_\alpha = \sqrt{\frac{2}{3}} v_a + (R_{f1} + 2R_{f2}) i_\alpha \quad (27)$$

$$v_\beta = R_{f1} i_\beta \quad (28)$$

$$v_0 = \frac{1}{\sqrt{3}} v_a + (R_{f1} + 2R_{f2}) i_0 \quad (29)$$

Therefore, the α and 0 circuits can be represented as coupled circuits through an ideal transformer with turn ratio $n = \sqrt{2}$, whereas the β circuit is uncoupled and loaded with the fault resistor R_{f1} (see Figure 9).

Notice that in this case the transient involves all the three components $\alpha\beta 0$. Moreover, fault grounding results in circuit coupling between α and 0 circuits.

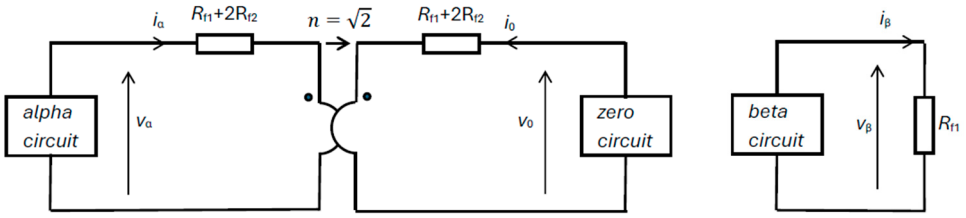

Figure 9. Equivalent circuits in the Clarke domain for the double-phase grounded fault.

3.2.1. Ungrounded Double-Phase Fault

In the special case of ungrounded double-phase fault, the fault resistor R_{f2} in Figure 8 is replaced by an open circuit (see Figure 10).

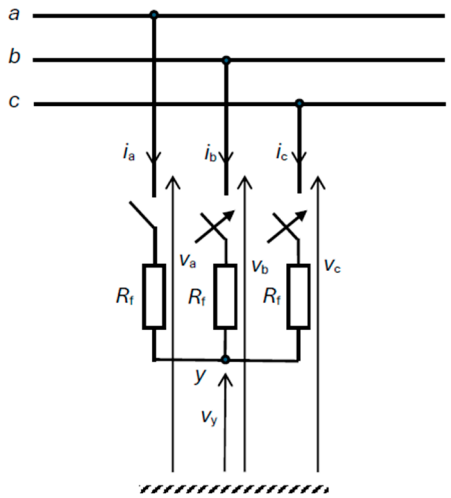

Figure 10. Circuit representation of double-phase ungrounded faults. By closing only the switches *b* and *c* the corresponding two phases are involved in the fault.

By taking into account the current constraint $i_a = i_y = 0$ we can write:

$$i_c = -i_b \quad (30)$$

Thus, the phase voltages in this case are given by:

$$v_a = v_{ay} + v_y$$

 doi:10.20944/preprints202605.0003.v2

$$v_b = v_{by} + v_y = R_f i_b + v_y \qquad (31)$$
$$v_c = v_{cy} + v_y = -R_f i_b + v_y$$

By using (30)-(31) into the Clarke transformation defined in (1), we can readily obtain the αβ0 voltages and currents:

$$\boldsymbol{v}_{\alpha\beta 0} = \begin{bmatrix} v_\alpha \\ v_\beta \\ v_0 \end{bmatrix} = \sqrt{\frac{2}{3}} \begin{bmatrix} 1 & -\frac{1}{2} & -\frac{1}{2} \\ 0 & \frac{\sqrt{3}}{2} & -\frac{\sqrt{3}}{2} \\ \frac{1}{\sqrt{2}} & \frac{1}{\sqrt{2}} & \frac{1}{\sqrt{2}} \end{bmatrix} \begin{bmatrix} v_{ay} + v_y \\ R_f i_b + v_y \\ -R_f i_b + v_y \end{bmatrix} = \sqrt{\frac{2}{3}} \begin{bmatrix} v_{ay} \\ \sqrt{3} R_f i_b \\ \frac{1}{\sqrt{2}} (v_{ay} + 3v_y) \end{bmatrix} \qquad (32)$$

$$\boldsymbol{i}_{\alpha\beta 0} = \begin{bmatrix} i_\alpha \\ i_\beta \\ i_0 \end{bmatrix} = \sqrt{\frac{2}{3}} \begin{bmatrix} 1 & -\frac{1}{2} & -\frac{1}{2} \\ 0 & \frac{\sqrt{3}}{2} & -\frac{\sqrt{3}}{2} \\ \frac{1}{\sqrt{2}} & \frac{1}{\sqrt{2}} & \frac{1}{\sqrt{2}} \end{bmatrix} \begin{bmatrix} 0 \\ i_b \\ -i_b \end{bmatrix} = \sqrt{\frac{2}{3}} \begin{bmatrix} 0 \\ \sqrt{3} i_b \\ 0 \end{bmatrix} \qquad (33)$$

Notice that v_α and v_β are not dependent on v_y. Moreover, since $i_\alpha = i_0 = 0$, the α and 0 circuits are open circuits, whereas the β circuit is closed on the fault resistor R_f, such that (see Figure 11):

$$v_\beta = R_f i_\beta \qquad (34)$$

as in the grounded fault case (28). Thus, in the ungrounded double-phase fault the transient involves only the β circuit. This is the opposite behavior of the single-phase fault described in Subsection 3.1. The α and 0 circuits remain in the steady-state open-circuit condition, therefore they can be readily solved as transient-free circuits.

Once i_β is calculated by solving the transient β circuit, from (33) i_b can be recovered as $i_b = i_\beta/\sqrt{2}$. Moreover, the phase voltages can be recovered from the inverse Clarke transformation (21).

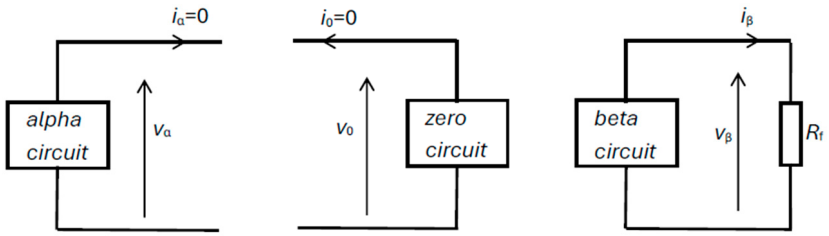

Figure 11. Equivalent circuits in the Clarke domain for the double-phase ungrounded fault.

3.3. Three-Phase Ungrounded Faults

A three-phase ungrounded fault can be modeled as in Figure 12. Fault asymmetry is implemented by assuming the phase *a* fault resistance R_{f1} as different from the fault resistances R_f of phases *b* and *c*. Thus, the phase voltages are given by:

$$v_a = R_{f1} i_a + v_y, \quad v_b = R_f i_b + v_y, \quad v_c = R_f i_c + v_y \qquad (35)$$

where the following current constraint must be considered:

$$i_a + i_b + i_c = 0 \qquad (36)$$

By using (35)-(36) into the Clarke transformation defined in (1), we can readily obtain the αβ0 voltages and currents:

$$\boldsymbol{v}_{\alpha\beta 0} = \begin{bmatrix} v_\alpha \\ v_\beta \\ v_0 \end{bmatrix} = \sqrt{\frac{2}{3}} \begin{bmatrix} 1 & -\frac{1}{2} & -\frac{1}{2} \\ 0 & \frac{\sqrt{3}}{2} & -\frac{\sqrt{3}}{2} \\ \frac{1}{\sqrt{2}} & \frac{1}{\sqrt{2}} & \frac{1}{\sqrt{2}} \end{bmatrix} \begin{bmatrix} R_{f1} i_a + v_y \\ R_f i_b + v_y \\ R_f i_c + v_y \end{bmatrix} = \sqrt{\frac{2}{3}} \begin{bmatrix} \left(R_{f1} + \frac{1}{2} R_f\right) i_a \\ \frac{\sqrt{3}}{2} R_f (i_b - i_c) \\ \frac{1}{\sqrt{2}} (R_{f1} - R_f) i_a + \frac{3}{\sqrt{2}} v_y \end{bmatrix} \qquad (37)$$

$$\boldsymbol{i}_{\alpha\beta 0} = \begin{bmatrix} i_\alpha \\ i_\beta \\ i_0 \end{bmatrix} = \sqrt{\frac{2}{3}} \begin{bmatrix} 1 & -\frac{1}{2} & -\frac{1}{2} \\ 0 & \frac{\sqrt{3}}{2} & -\frac{\sqrt{3}}{2} \\ \frac{1}{\sqrt{2}} & \frac{1}{\sqrt{2}} & \frac{1}{\sqrt{2}} \end{bmatrix} \begin{bmatrix} i_a \\ i_b \\ i_c \end{bmatrix} = \sqrt{\frac{2}{3}} \begin{bmatrix} \frac{3}{2} i_a \\ \frac{\sqrt{3}}{2} (i_b - i_c) \\ 0 \end{bmatrix} \qquad (38)$$

Notice that v_α and v_β are not dependent on v_y. Moreover, since from (38) we obtain:

 doi:10.20944/preprints202605.0003.v2

$$i_\alpha = \sqrt{\frac{3}{2}} i_a, \quad i_\beta = \frac{1}{\sqrt{2}}(i_b - i_c), \quad i_0 = 0 \quad (39)$$

from (37) the following $\alpha\beta 0$ relationships can be derived:

$$v_\alpha = \frac{2}{3}\left(R_{f1} + \frac{1}{2}R_f\right) i_\alpha \quad (40)$$

$$v_\beta = R_f i_\beta \quad (41)$$

$$i_0 = 0 \quad (42)$$

Thus, the α and β circuits are uncoupled, whereas the 0 circuit is open (i.e., $i_0 = 0$) (see Figure 13).

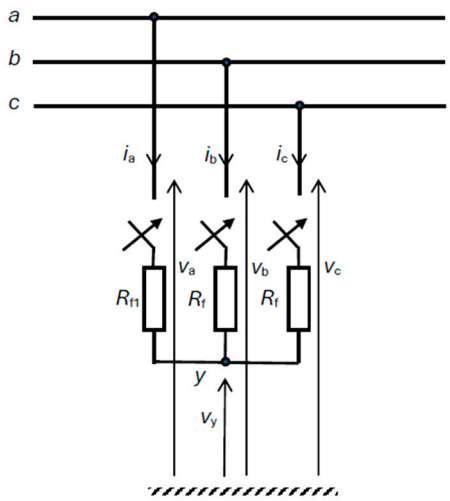

Figure 12. Circuit representation of three-phase ungrounded asymmetrical faults. Asymmetry is taken into account by assuming $R_{f1} \neq R_f$.

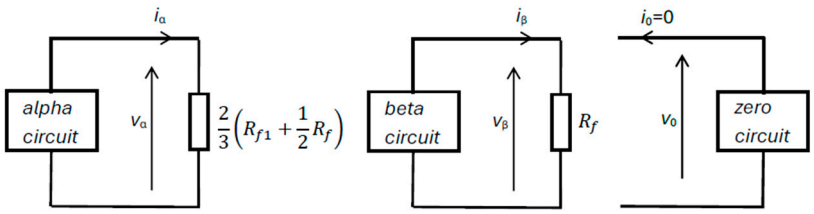

Figure 13. Equivalent circuits in the Clarke domain for the three-phase ungrounded asymmetrical fault.

Notice that the three-phase transient can be solved as the two independent transients of α and β circuits. In the special case of symmetric fault, i.e. $R_{f1} = R_f$, from (40)-(41) we obtain that the load of the α circuit equals the load of the β circuit.

Once the $\alpha\beta 0$ circuits in Figure 13 are solved, the *abc* phase voltages can be recovered through the inverse Clarke transformation as in (21). Similarly, the *abc* currents can be recovered as:

$$\boldsymbol{i}_{abc} = \begin{bmatrix} i_a \\ i_b \\ i_c \end{bmatrix} = \sqrt{\frac{2}{3}} \begin{bmatrix} 1 & 0 & \frac{1}{\sqrt{2}} \\ -\frac{1}{2} & \frac{\sqrt{3}}{2} & \frac{1}{\sqrt{2}} \\ -\frac{1}{2} & -\frac{\sqrt{3}}{2} & \frac{1}{\sqrt{2}} \end{bmatrix} \begin{bmatrix} i_\alpha \\ i_\beta \\ 0 \end{bmatrix} = \sqrt{\frac{2}{3}} \begin{bmatrix} Re\{\bar{\imath}\} \\ Re\{a^2\bar{\imath}\} \\ Re\{a\bar{\imath}\} \end{bmatrix} \quad (43)$$

where $\bar{\imath} = i_\alpha + j i_\beta$ is the current space vector. Notice that, according to (42), the contribution of i_0 in (43) is null.

4. Numerical Validation

The analytical results derived in Section 3 were validated through the numerical simulation in Matlab/Simscape of the simple radial system depicted in Figure 14.

 doi:10.20944/preprints202605.0003.v2

The equivalent balanced generator connected at bus 1 (including transformer contribution) is characterized by a 60 Hz phase voltage equal to $1/\sqrt{2}$ kV, positive/negative reactance $X_g = 0.5\ \Omega$ and resistance $R_g = 0.1\ \Omega$, zero sequence reactance $X_{0g} = 0.25\ \Omega$, and grounding reactance $X_{gr} = 0.2\ \Omega$. The line is modeled with positive/negative sequence reactance $X_{line} = 0.3\ \Omega$/km and resistance $R_{line} = 0.1\ \Omega$/km, and zero sequence reactance $X_{0line} = 0.9\ \Omega$/km. The fault is located at distance d from bus 1. Negligible load currents were assumed during the fault transient.

The four fault cases analyzed in Section 3 were implemented by assuming fault locations d and fault resistance R_f as parameters. For each case, the transient currents at fault location and the locus of the voltage space vector at bus 1 were evaluated and plotted. Analytical and numerical results were always overlapping, therefore in the following figures no distinction has been made between analytical and numerical curves.

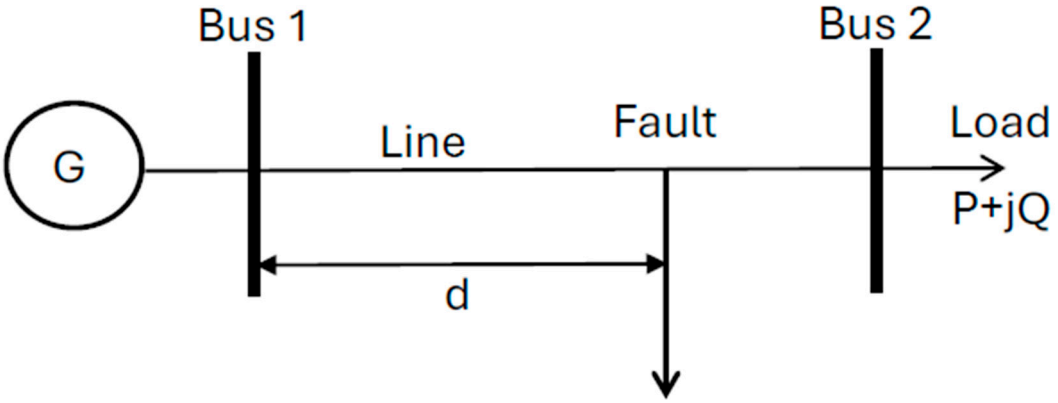

Figure 14. Radial system used to validate the analytical results. The fault location is at distance d from the bus 1.

4.1. Single-Phase Faults

Single-phase faults, described in Subsection 3.1, have been implemented in Matlab/Simscape in order to validate the analytical results. In particular, the current i_α and the corresponding fault current i_a were evaluated at fault location $d = 10$ km for two different values of fault resistance, i.e., $R_f = 0$ and $R_f = 1\ \Omega$ (see Figure 15). Clearly, a lower value of R_f results in larger excursion of the fault current and a larger time constant. This behavior is more evident in Figure 16 where the fault location is $d = 1$ km. Indeed, in this case the line parameters have lower impact, and therefore the fault current has a larger excursion in case of fault with zero resistance.

Figure 17 shows the phase voltages v_{abc} at fault location $d = 10$ km for fault resistance $R_f = 0$. Overvoltage of unfaulted phases b and c is evident,

Figure 18 shows the behavior of the voltage space vector at bus 1 in case of fault with $R_f = 0$. The black curve shows the circular ideal trajectory in case of no fault. The blue curve shows the trajectory in case of fault location $d = 10$ km, whereas the red curve shows the trajectory in case of fault location $d = 1$ km. Clearly, at smaller distance the detection of the single-phase fault becomes more evident, since the elliptical trajectory with inclination angle 90° can be readily detected. Figure 19 shows the voltage space vector in the case of fault with $R_f = 1\ \Omega$. Notice that the fault resistance results in a slight deviation of the ellipse inclination, and a smaller difference between $d = 1$ km and $d = 10$ km. Thus, as it was expected, faults with larger resistance result in lower detection capability of the space vector trajectory. The apparent double red curve is due to the transient behavior.

 doi:10.20944/preprints202605.0003.v2

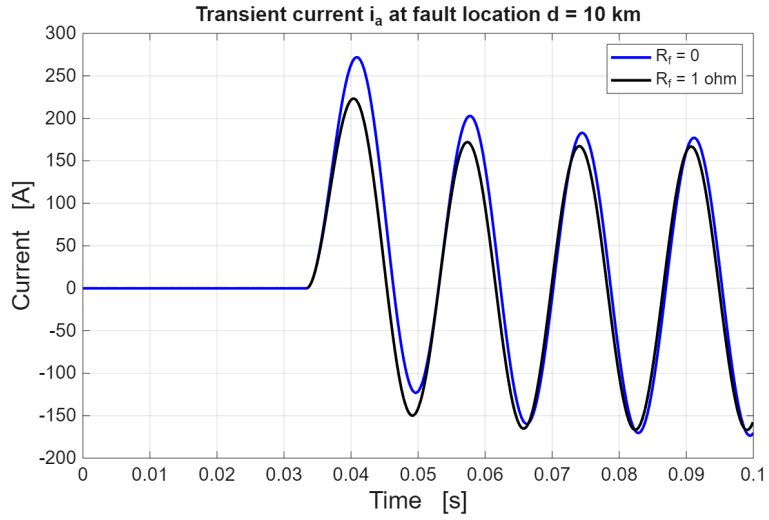

Figure 15. Transient behavior of the phase current i_a for a single-phase fault after two cycles at 60 Hz. The location of the fault is $d = 10$ km from the bus 1, and two different values for the fault resistance are considered.

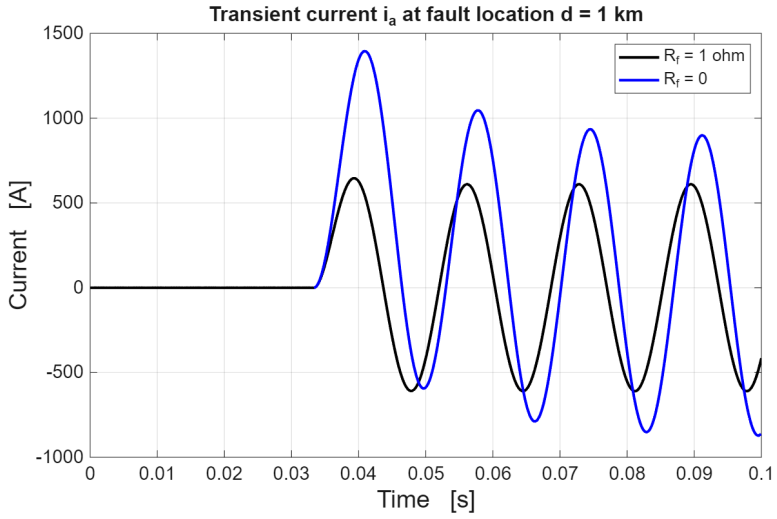

Figure 16. Transient behavior of the phase current i_a for a single-phase fault after two cycles at 60 Hz. The location of the fault is $d = 1$ km from the bus 1, and two different values for the fault resistance are considered.

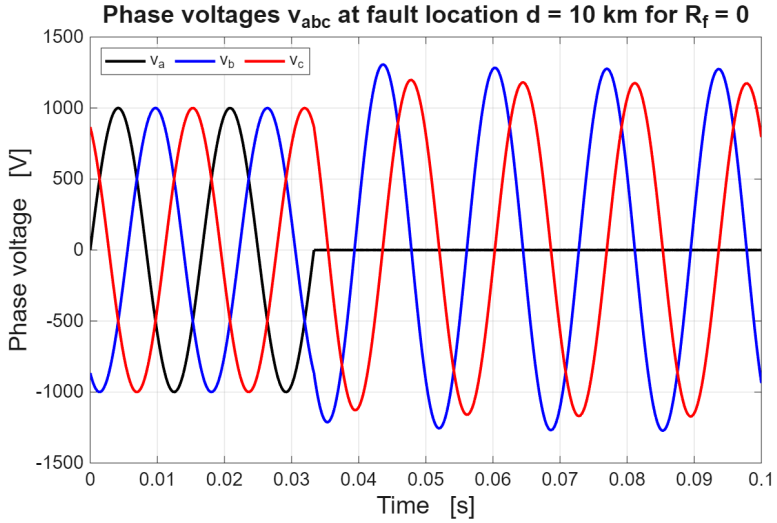

Figure 17. Transient behavior of the phase voltages v_{abc} for a single-phase fault with $R_f = 0$ after two cycles at 60 Hz. The location of the fault is $d = 10$ km from the bus 1.

 doi:10.20944/preprints202605.0003.v2

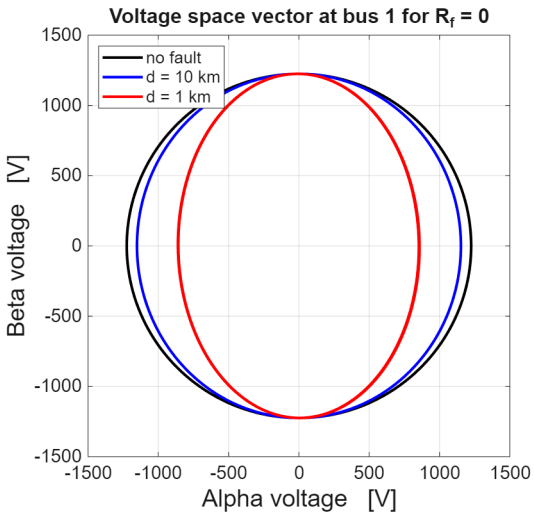

Figure 18. Trajectory of the voltage space vector at bus 1 in case of fault resistance $R_f = 0$. The black curve corresponds to the ideal circular trajectory in case of no fault. The blue trajectory was obtained for a fault location $d = 10$ km, whereas the red trajectory corresponds to fault location $d = 1$ km.

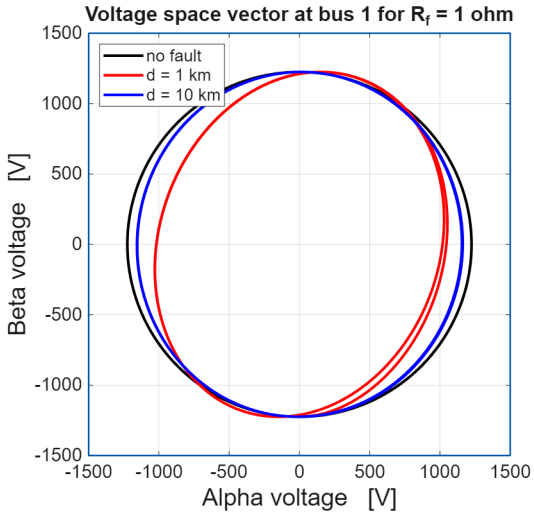

Figure 19. Trajectory of the voltage space vector at bus 1 in case of fault resistance $R_f = 1\,\Omega$. The black curve corresponds to the ideal circular trajectory in case of no fault. The blue trajectory was obtained for a fault location $d = 10$ km, whereas the red trajectory corresponds to fault location $d = 1$ km.

4.2. Double-Phase Grounded Faults

Double-phase grounded faults, described in Subsection 3.2, have been implemented in Matlab/Simscape in order to validate the analytical results. In particular, the currents i_α and i_β, and the corresponding fault current $(i_b + i_c)$ were evaluated at fault location $d = 10$ km for two different values of fault resistance, i.e., $R_{f2} = 0$ and $R_{f2} = 1\,\Omega$, while it was kept $R_{f1} = 0$ (see Figure 20). A lower value of R_{f2} results in larger excursion of the fault current and a larger time constant. This behavior is more evident in Figure 21 where the fault location is $d = 1$ km. Indeed, in this case the line parameters have lower impact, and therefore the fault current has a larger excursion in case of fault with zero resistance.

Figure 22 shows the behavior of the voltage space vector at bus 1 in case of fault with $R_{f2} = 0$. The black curve shows the circular ideal trajectory in case of no fault. The blue curve shows the trajectory in case of fault location $d = 10$ km, whereas the red curve shows the trajectory in case of fault location $d = 1$ km. Clearly, at smaller distance the detection of the double-phase fault becomes more evident, since the elliptical trajectory with inclination angle 0° can be readily detected. Figure

 doi:10.20944/preprints202605.0003.v2

23 shows the voltage space vector in the case of fault with $R_{f2} = 1\ \Omega$. Notice that, according to the analytical results, the fault resistance R_{f2} affects only α component, not the β component. In fact, the red curves in Figures 22 and 23 have a different horizontal excursion, but they keep the same vertical excursion. The detection capability of the space vector trajectory remains effective since the phase-to-phase fault resistance R_{f1} is kept to zero.

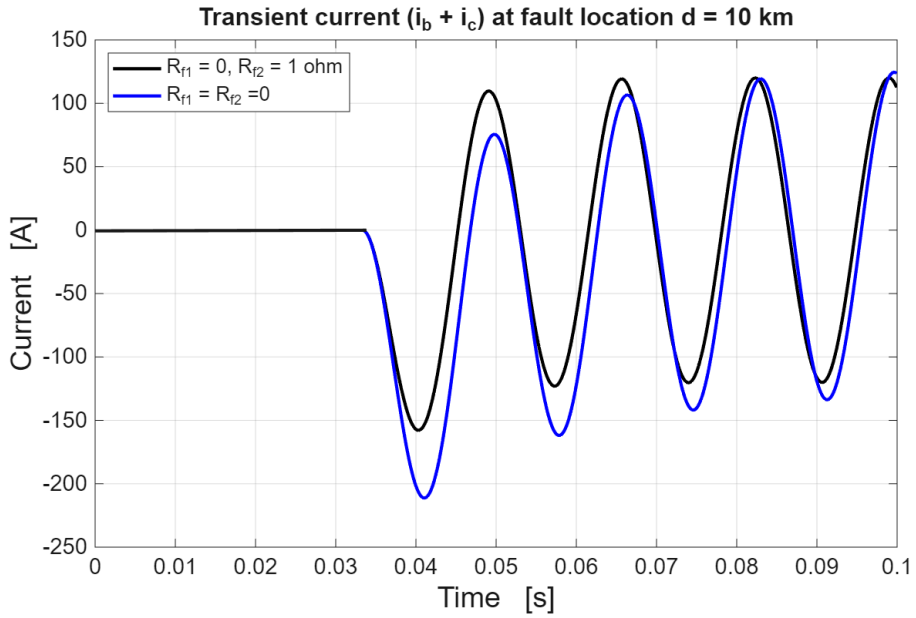

Figure 20. Transient behavior of the fault current $(i_b + i_c)$ for a grounded double-phase fault after two cycles at 60 Hz. The location of the fault is $d = 10$ km from the bus 1, and two different values for the fault resistance R_{f2} are considered.

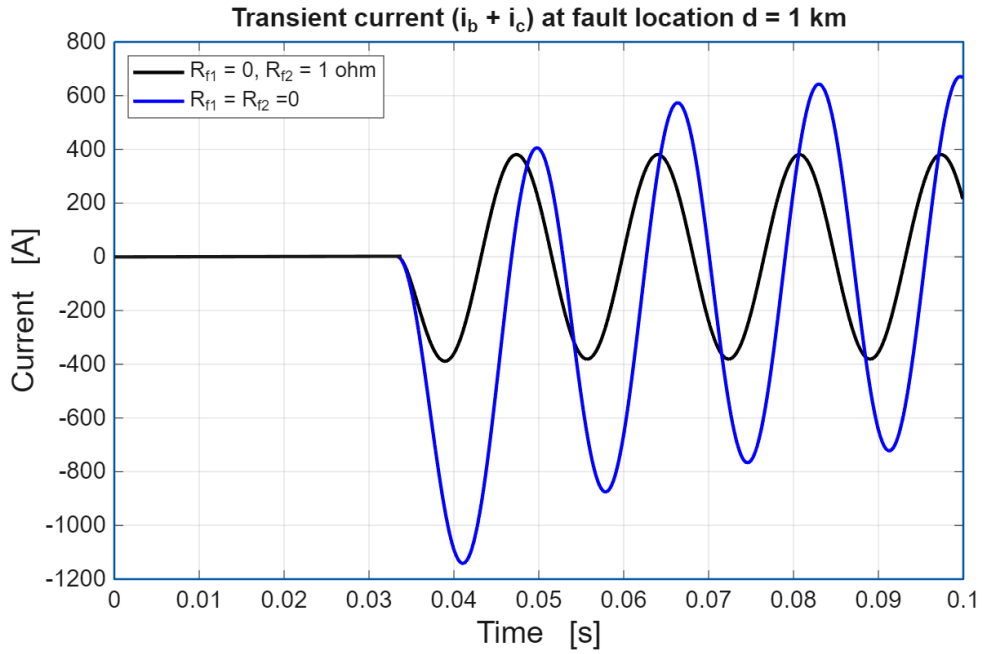

Figure 21. Transient behavior of the fault current $(i_b + i_c)$ for a grounded double-phase fault after two cycles at 60 Hz. The location of the fault is $d = 1$ km from the bus 1, and two different values for the fault resistance R_{f2} are considered.

 doi:10.20944/preprints202605.0003.v2

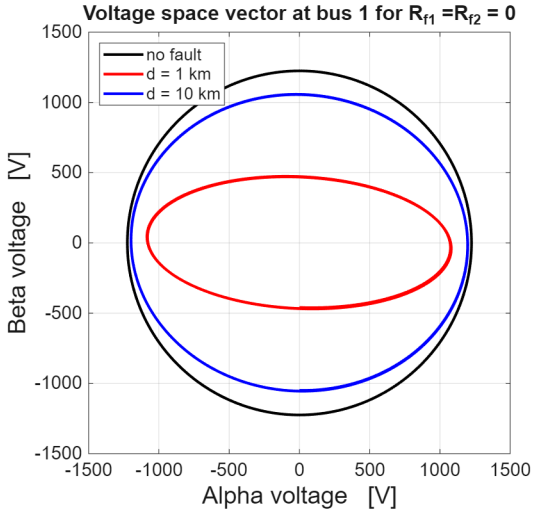

Figure 22. Trajectory of the voltage space vector at bus 1 in case of fault resistances $R_{f1} = R_{f2} = 0$. The black curve corresponds to the ideal circular trajectory in case of no fault. The blue trajectory was obtained for a fault location $d = 10$ km, whereas the red trajectory corresponds to fault location $d = 1$ km.

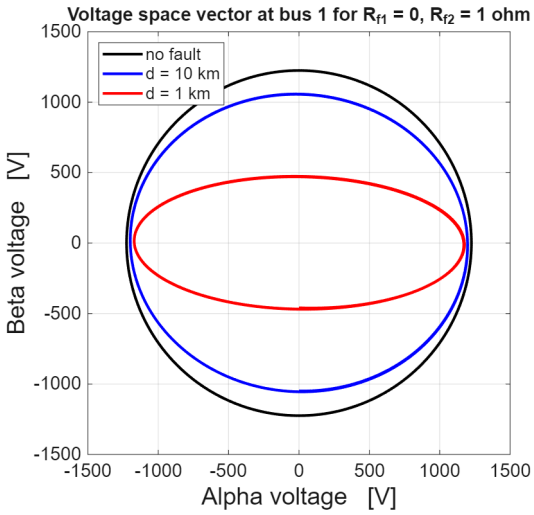

Figure 23. Trajectory of the voltage space vector at bus 1 in case of fault resistances $R_{f1} = 0$, $R_{f2} = 1\ \Omega$. The black curve corresponds to the ideal circular trajectory in case of no fault. The blue trajectory was obtained for a fault location $d = 10$ km, whereas the red trajectory corresponds to fault location $d = 1$ km.

4.3. Double-Phase Ungrounded Faults

Double-phase ungrounded faults, described in Subsection 3.2.1, have been implemented in Matlab/Simscape in order to validate the analytical results. In particular, the currents i_β and the corresponding fault current $i_b = i_\beta/\sqrt{2}$ were evaluated at fault location $d = 10$ km for two different values of fault resistance, i.e., $R_f = 0$ and $R_f = 1\ \Omega$ (see Figure 24). A lower value of R_f results in larger excursion of the fault current and a larger time constant. This behavior is more evident in Figure 25 where the fault location is $d = 1$ km. Indeed, in this case the line parameters have lower impact, and therefore the fault current has a larger excursion in case of fault with zero resistance.

Figure 26 shows the behavior of the voltage space vector at bus 1 in case of fault with $R_f = 0$. The black curve shows the circular ideal trajectory in case of no fault. The blue curve shows the trajectory in case of fault location $d = 10$ km, whereas the red curve shows the trajectory in case of fault location $d = 1$ km. Clearly, at smaller distance the detection of the double-phase fault becomes more evident, since the elliptical trajectory with inclination angle 0° can be readily detected. Figure 27 shows the voltage space vector in the case of fault with $R_f = 1\ \Omega$. Notice that, according to the

 doi:10.20944/preprints202605.0003.v2

analytical results, the fault resistance R_f affects only the β component, not the α component. In fact, the red curves in Figures 26 and 27 have a different vertical excursion, but they keep the same horizontal excursion. Notice that the fault resistance results in a slight deviation of the ellipse inclination, and a smaller difference between $d = 1$ km and $d = 10$ km. Thus, as it was expected, faults with larger resistance result in lower detection capability of the space vector trajectory. The transient behavior is also evident in the blue and red curves.

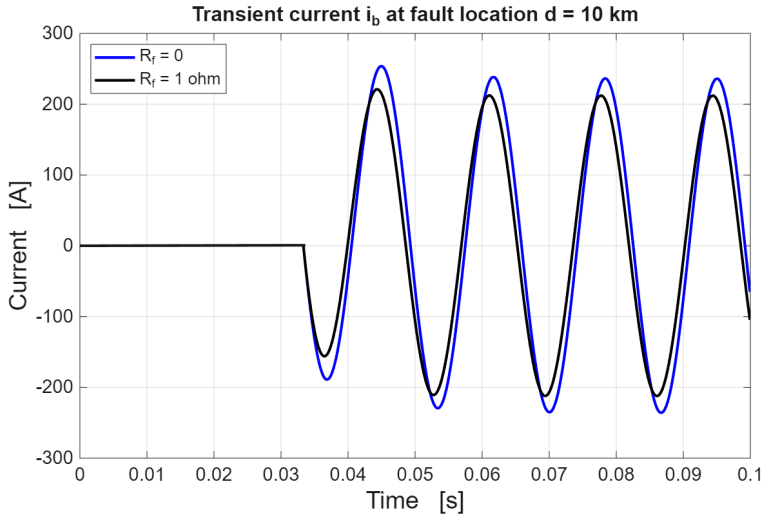

Figure 24. Transient behavior of the phase current i_b for a double-phase ungrounded fault after two cycles at 60 Hz. The location of the fault is $d = 10$ km from the bus 1, and two different values for the fault resistance are considered.

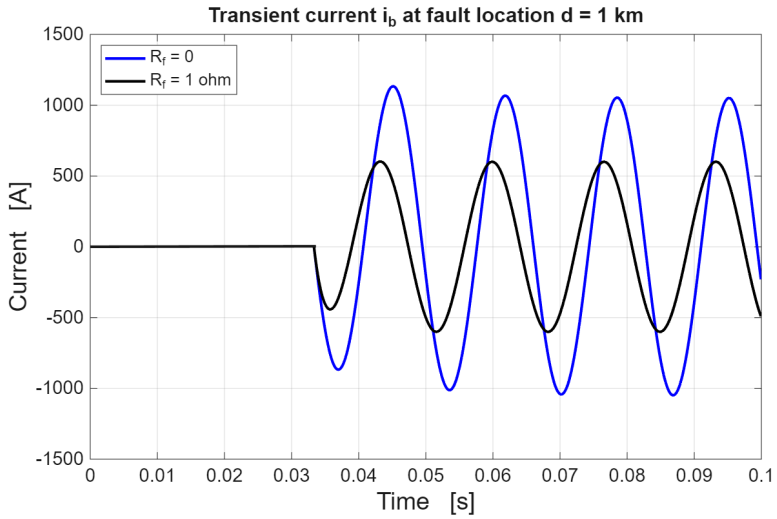

Figure 25. Transient behavior of the phase current i_b for a double-phase ungrounded fault after two cycles at 60 Hz. The location of the fault is $d = 1$ km from the bus 1, and two different values for the fault resistance are considered.

 doi:10.20944/preprints202605.0003.v2

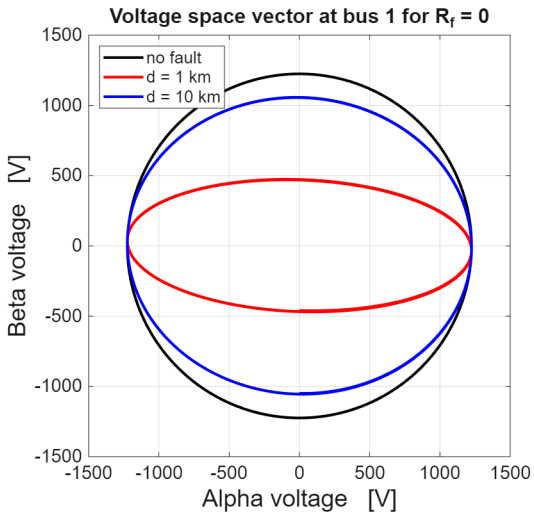

Figure 26. Trajectory of the voltage space vector at bus 1 in case of fault resistance $R_f = 0$. The black curve corresponds to the ideal circular trajectory in case of no fault. The blue trajectory was obtained for a fault location $d = 10$ km, whereas the red trajectory corresponds to fault location $d = 1$ km.

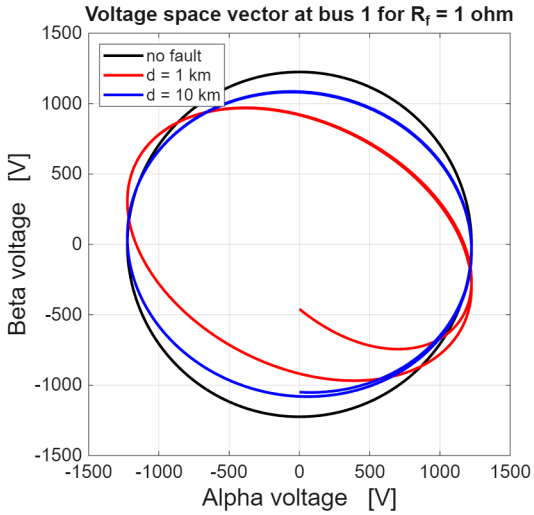

Figure 27. Trajectory of the voltage space vector at bus 1 in case of fault resistance $R_f = 1\ \Omega$. The black curve corresponds to the ideal circular trajectory in case of no fault. The blue trajectory was obtained for a fault location $d = 10$ km, whereas the red trajectory corresponds to fault location $d = 1$ km.

4.4. Three-Phase Ungrounded Faults

Three-phase ungrounded faults, described in Subsection 3.3, have been implemented in Matlab/Simscape in order to validate the analytical results. In particular, the currents i_α and i_β, and the corresponding fault current $i_a = i_\alpha\sqrt{2/3}$ were evaluated at fault location $d = 10$ km for two different values of fault resistance, i.e., $R_{f1} = 0.1\ \Omega$ and $R_{f1} = 1\ \Omega$, while R_f was kept equal to zero (see Figure 28). A lower value of R_{f1} results in larger excursion of the fault current and a larger time constant. This behavior is more evident in Figure 29 where the fault location is $d = 1$ km. Indeed, in this case the line parameters have lower impact, and therefore the fault current has a larger excursion in case of fault with zero resistance.

Figure 30 shows the behavior of the voltage space vector at bus 1 in case of fault with $R_{f1} = 0.1\ \Omega$ and $R_f = 0$. The black curve shows the circular ideal trajectory in case of no fault. The blue curve shows the trajectory in case of fault location $d = 10$ km, whereas the red curve shows the trajectory in case of fault location $d = 1$ km. The transient behavior is also evident in red curve.

 doi:10.20944/preprints202605.0003.v2

Figure 31 shows the voltage space vector in the case of fault with $R_{f1} = 1\,\Omega$. Notice that, according to the analytical results, the fault resistance R_{f1} affects only the α component, not the β component. In fact, the red curves in Figures 30 and 31 have a different horizontal excursion, but they keep the same vertical excursion. Notice that the increase in the fault resistance results in elliptical behavior instead of the almost circular behavior in Figure 30. The transient behavior is also evident in the red curve.

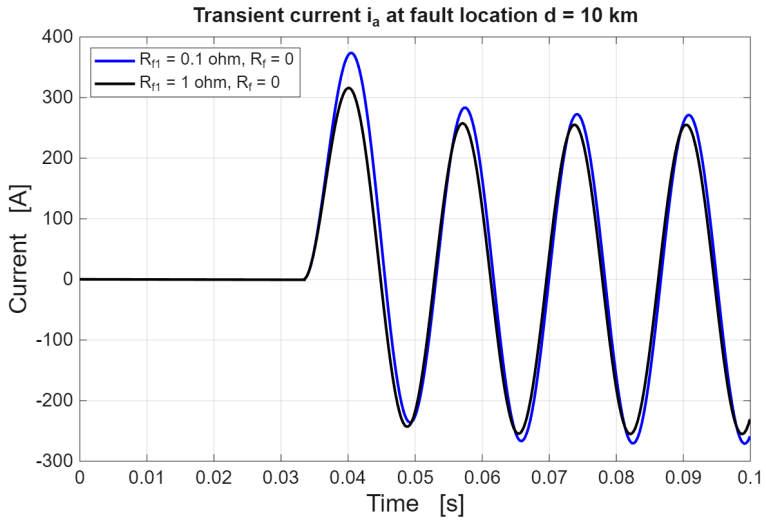

Figure 28. Transient behavior of the phase current i_a for a three-phase ungrounded fault after two cycles at 60 Hz. The location of the fault is $d = 10$ km from the bus 1, and two different values for the fault resistance are considered.

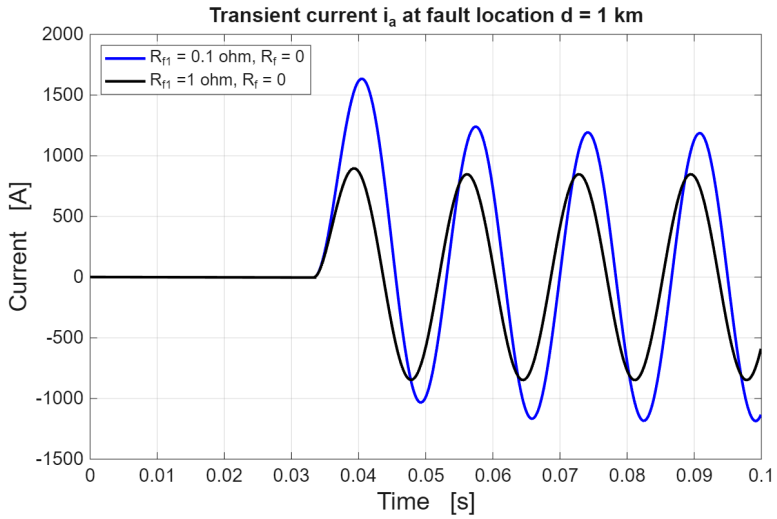

Figure 29. Transient behavior of the phase current i_a for a three-phase ungrounded fault after two cycles at 60 Hz. The location of the fault is $d = 1$ km from the bus 1, and two different values for the fault resistance are considered.

 doi:10.20944/preprints202605.0003.v2

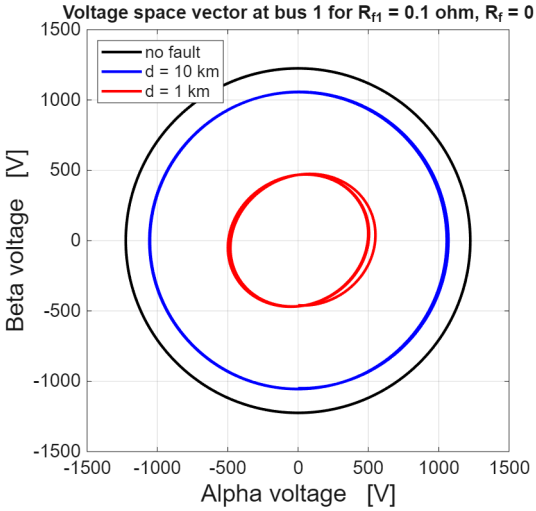

Figure 30. Trajectory of the voltage space vector at bus 1 in case of fault resistance $R_{f1} = 0.1\,\Omega$. The black curve corresponds to the ideal circular trajectory in case of no fault. The blue trajectory was obtained for a fault location $d = 10$ km, whereas the red trajectory corresponds to fault location $d = 1$ km.

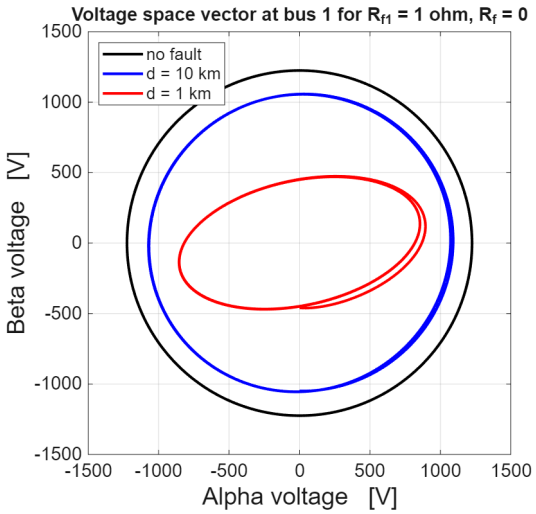

Figure 31. Trajectory of the voltage space vector at bus 1 in case of fault resistance $R_{f1} = 1\,\Omega$. The black curve corresponds to the ideal circular trajectory in case of no fault. The blue trajectory was obtained for a fault location $d = 10$ km, whereas the red trajectory corresponds to fault location $d = 1$ km.

5. Conclusions

The proposed Clarke-transformation approach for time-domain analysis of asymmetrical faults in three-phase systems was successfully validated by numerical simulation of a faulted radial system. The time-domain analytical results overlap exactly with the numerical results. Thus, the proposed approach provides the rigorous analytical solution of three-phase transients even in case of asymmetrical faults.

Future work will be devoted to extend the proposed methodology to simultaneous faults and phase interruptions.

Funding: This research received no external funding.

Conflicts of Interest: The author declares no conflict of interest.

References

1. Tleis, N. *Power Systems Modeling and Fault Analysis*, 2nd ed., Academic Press, Elsevier, 2019.

 doi:10.20944/preprints202605.0003.v2

2. Martinez-Velasco, J.A. *Transient Analysis of Power Systems,* John Wiley & Sons, Ltd, 2015.
3. Zanetta Jr., L.C. Understanding Electromagnetic Transients in Power Systems, IEEE Press, 2025.
4. Bellan, D.; Superti-Furga, G. Space-vector state-equation analysis of three-phase transients. *Journal of Electrical Systems* **2018**, *Vol. 14*, pp. 188-198.
5. Bellan, D. Clarke transformation solution of asymmetrical transients in three-phase circuits. *Energies* **2020**, *Vol. 13*, pp. 1-19.
6. Bellan, D. Analytical investigation of the properties of transients in unbalanced three-phase four-wire networks. *Energies* **2022**, *Vol. 15*, pp. 1-26.
7. Ignatova, V.; Granjon, P.; Bacha, S. Space vector method for voltage dips and swells analysis. *IEEE Trans. on Power Delivery* **2009**, *Vol. 24*, pp. 2054-2061.
8. M. R. Alam, K.M.Muttaqi, and A. Bouzerdoum, Characterizing voltage sags and swells using three-phase voltage ellipse parameters. *IEEE Trans. Ind. Appl*. **2015**, *Vol. 51*, pp. 2780-2790.
9. J. R. Camarillo-Peñaranda and G. Ramos, Fault classification and voltage sag parameter computation using voltage ellipses. *IEEE Trans. Ind. Appl*. **2019**, *Vol. 55*, pp. 92-97.
10. J. R. Camarillo-Peñaranda and G. Ramos, Characterization of voltage sags due to faults in radial systems using three-phase voltage ellipse parameters. *IEEE Trans. Ind. Appl*. **2018**, *Vol. 54*, pp. 2032-2040.
11. T. García-Sánchez, E. Gómez-Lázaro, E. Muljadi, M. Kessler, A. Molina-García, Approach to fitting parameters and clustering for characterizing measured voltage dips based on two-dimensional polarisation ellipses. *Renewable Power Generation IET* **2017**, *Vol. 11*, pp. 1335-1343.
12. Bagheri, A.; Bollen, M.H.J. Space phasor model-based monitoring of voltages in three-phase systems. In Proc. 18th International Conference on Harmonics and Quality of Power (ICHQP), 2018.
13. Li, S.; Xie, L.; Liu, Y. Fast Identification Method for Voltage Sag Type and Characteristic. In Proc. IECON 2019 - 45th Annual Conference of the IEEE Industrial Electronics Society, Lisbon, Portugal, 2019.
14. Bagheri, A.; Bollen, M.H.J.; Gu, I.Y.H. Improved characterization of multi-stage voltage dips based on the space phasor model. *Electric Power Systems Research* **2018**, *Vol. 154*, pp. 319.
15. Alam, M.R.; Muttaqi, K.M.; Bouzerdoum, A. A new approach for classification and characterization of voltage dips and swells using 3-D polarization ellipse parameters. *IEEE Trans. Power Del.* **2015**, *Vol. 30*, pp. 1344-1353.
16. Alam, M.R.; Muttaqi, K.M.; Saha, T.K. Classification and Localization of Fault-Initiated Voltage Sags Using 3-D Polarization Ellipse Parameters. *IEEE Transactions on Power Delivery* **2020**, *Vol. 35*, pp. 1812-1822.
17. Bellan, D. Probability Density Function of Three-Phase Ellipse Parameters for the Characterization of Noisy Voltage Sags. *IEEE Access* **2020**, *Vol. 8*, pp. 185503-185513.
18. Bellan, D. Clarke Circuit Analysis for Space-Vector Ellipse Characterization of Phase-to-Ground Faults in Three-Phase Radial Systems. *WSEAS Transactions on Circuits and Systems* **2023**, *Vol. 22*, pp. 243–250.